Analytic Quantification of Bias and Variance of Coil Sensitivity Profile Estimators for Improved Image Reconstruction in MRI*

Aymeric Stamm, Jolene Singh, Onur Afacan, and Simon K. Warfield

CRL - Boston Children's Hospital, Harvard Medical School, MA, USA
aymeric.stamm@childrens.harvard.edu

Abstract. Magnetic resonance (MR) imaging provides a unique in-vivo capability of visualizing tissue in the human brain non-invasively, which has tremendously improved patient care over the past decades. However, there are still prominent artifacts, such as intensity inhomogeneities due to the use of an array of receiving coils (RC) to measure the MR signal or noise amplification due to accelerated imaging strategies. It is critical to mitigate these artifacts for both visual inspection and quantitative analysis. The cornerstone to address this issue pertains to the knowledge of coil sensitivity profiles (CSP) of the RCs, which describe how the measured complex signal decays with the distance to the RC.

Existing methods for CSP estimation share a number of limitations: (i) they primarily focus on CSP magnitude, while it is known that the solution to the MR image reconstruction problem involves complex CSPs and (ii) they only provide point estimates of the CSPs, which makes the task of optimizing the parameters and acquisition protocol for their estimation difficult. In this paper, we propose a novel statistical framework for estimating complex-valued CSPs. We define a CSP estimator that uses spatial smoothing and additional body coil data for phase normalization. The main contribution is to provide detailed information on the statistical distribution of the CSP estimator, which yields automatic determination of the optimal degree of smoothing for ensuring minimal bias and provides guidelines to the optimal acquisition strategy.

Keywords: coil sensitivity profile, bias, variance, image reconstruction.

1 Introduction

A modern magnetic resonance (MR) scanner collects signal using an array of receiving surface coils (RSC) [5], from which an image reconstruction problem is solved to obtain the highest SNR composite image, which magnitude is of main interest for radiological evaluation. The coil sensitivity profile (CSP) is a spatially varying magnetic field generated by the RSC that characterizes how RSC signal magnitude and phase spatially vary. In most MRI applications, an array

* This work was supported in part by NIH Awards RO1 EB013248, RO1 NS079788, RO1 DK100404, RO1 EB019483 and 5R42 MH086984.

N. Navab et al. (Eds.): MICCAI 2015, Part II, LNCS 9350, pp. 684–691, 2015.
DOI: 10.1007/978-3-319-24571-3_82

of RSCs is used because it provides stronger MR signal near the coil location. On the other hand, RSC-measured signal rapidly decays with the distance to the coil and the signal phase is not as spatially homogeneous as with the RBC. Since RSCs are distributed around the coil array, conventional MR imaging suffers from a *shading artifact* that pertains to an important signal loss at the image center, impairing tissue contrast or abnormality detections. Moreover, a number of accelerated MRI acquisition strategies have been devised in the literature to enable the collection of more images in shorter scan times (see [2] for a comprehensive review). They rely on sub-sampling the k-space and resort to inferential procedures for recovering missing data, which represents an additional source of noise, called *g-factor noise*, that is strongly increased by poor CSP estimates.

A number of methods have already been proposed in the literature for addressing this problem (see [10] for a detailed review). With the latest methods emerged the idea of using the RBC measurement to help with the CSP estimation of RSCs. For instance, Siemens online reconstruction offers the possibility to compensate for intensity inhomogeneity via the method proposed in [3], which define the CSP estimator as the ratio of the two low-pass filtered magnitude images measured by the RSC and RBC respectively. In our opinion, these state-of-the art methods present two major limitations. First, they primarily focus on the magnitude of the CSPs, while neglecting phase variations, while it is known that the linear combination of RSC images that yields highest SNR composite image involves complex-valued weights that depend on (i) the real-valued covariance structure of the coil array and (ii) the complex-valued CSPs [9]. Second, they only provide a voxelwise point estimate of the CSPs, while ignoring the distribution of the underlying CSP estimator, which is of critical importance to reason about the choice of the parameters of such estimators or the optimal acquisition strategy to ensure consistent CSP estimates.

The scope of this work is to provide a novel statistical framework for the estimation of complex-valued CSPs. In the same line as [3], the CSP estimator that we aim at studying uses low-pass filtered RSC and RBC images, where the RBC measurement enables phase normalization to mitigate phase-variation artifacts. The important difference with respect to [3]'s estimator resides in the use of complex images rather than their magnitude only and in RBC normalization only affecting the phase of the estimator. The focus is on understanding the statistical distribution of the proposed CSP estimator, for which we derive the analytic expression of bias and variance, which ultimately leads to the automatic determination of the optimal degree of smoothing for ensuring minimal bias. We apply this new approach to the image reconstruction problem. We provide a comparison of the reconstructed image using our CSP estimator, optimized via knowledge of its statistical distribution, and using the approach proposed by [3].

2 Theory

In the rest of the paper, $\boldsymbol{x}$ represents voxel locations. Straight, curved, bold and non-bold symbols designate random variables, fixed values, vectors and scalars, respectively. The upperscripts *, $^\top$ and ^{H} are the conjugate, transpose and conjugate transpose operators respectively.The symbols $\mathcal{M}$, $\mathcal{P}$, $\mathcal{R}$ and $\mathcal{I}$ denote respectively the magnitude, phase, real and imaginary operators for any complex number. Finally, τ, g and G are respectively the standard deviation, density and distribution functions of the standard Gaussian distribution.

Let $\mathbf{c}(\boldsymbol{x}) = (c_1(\boldsymbol{x}), \ldots, c_L(\boldsymbol{x}))^\top$ be the $\mathbb{C}^L$-valued random variable representing the complex signals measured by an array of L RSCs. Following [9], the linear combination of these signals that yields SNR-maximized signal $\mathrm{s}(\boldsymbol{x})$ is:

$$\mathrm{s}(\boldsymbol{x}) = \frac{\boldsymbol{b}^H(\boldsymbol{x})\Sigma^{-1}\mathbf{c}(\boldsymbol{x})}{\sqrt{\boldsymbol{b}^H(\boldsymbol{x})\Sigma^{-1}\boldsymbol{b}(\boldsymbol{x})}}\,, \tag{1}$$

where $\boldsymbol{b}(\boldsymbol{x})$ is the $\mathbb{C}^L$-valued vector of CSPs at voxel $\boldsymbol{x}$ and Σ is the $L \times L$ noise covariance structure of the coil array. The above equation can be rewritten more conveniently as $\mathrm{s}(\boldsymbol{x}) = \boldsymbol{\beta}^H(\boldsymbol{x})\Sigma^{-1/2}\mathbf{c}(\boldsymbol{x})$, where:

$$\boldsymbol{\beta}(\boldsymbol{x}) = \frac{\Sigma^{-1/2}\boldsymbol{b}(\boldsymbol{x})}{\sqrt{\boldsymbol{b}^H(\boldsymbol{x})\Sigma^{-1}\boldsymbol{b}(\boldsymbol{x})}}\,, \tag{2}$$

is the **normalized uncorrelated CSP** vector that we aim at estimating.

2.1 Noise Covariance Estimation

Let $\mathbf{c}(\boldsymbol{x})$ and $\mathrm{c}_0(\boldsymbol{x})$ be the $\mathbb{C}^L$-valued and $\mathbb{C}$-valued random variables, representing the complex signals measured by an array of L RSCs and by the RBC respectively at voxel $\boldsymbol{x}$. It is known that the random variable $\mathbf{c}(\boldsymbol{x})$ follows a multivariate complex Gaussian distribution [7]. When the full k-space is sampled, the covariance structure of the coil array can be assumed spatially-invariant [7].

For a voxel $\boldsymbol{x}_B$ in the background of the image, we have $\boldsymbol{c}(\boldsymbol{x}_B) = 0$. Hence, if N_B denotes the number of background voxels, we can thus think of the complex signals measured in the background as a set of $2N_B$ independent and identically distributed centered Gaussian variables with covariance Σ. The sample covariance estimator on background signals provides an unbiased estimate of Σ:

$$\Sigma = \frac{1}{2N_B - 1}\sum_{\boldsymbol{x}_B}\left[\mathcal{R}\left(\mathbf{c}(\boldsymbol{x}_B)\right)\mathcal{R}\left(\mathbf{c}(\boldsymbol{x}_B)\right)^\top + \mathcal{I}\left(\mathbf{c}(\boldsymbol{x}_B)\right)\mathcal{I}\left(\mathbf{c}(\boldsymbol{x}_B)\right)^\top\right]. \tag{3}$$

Since $N_B \gg 1$ in most MR images ($N_B \approx 2$ millions for a $2 \times 2 \times 2$ mm brain image), this estimator is almost noise-free. We thus assume, from now on, that Σ is completely known and computed via Eq. (3).

2.2 Coil Sensitivity Profile Estimation

The CSP of an RSC is the spatially-referenced map of magnetic field generated per unit current flowing through the RSC. MR physics principles states the following properties of CSPs:

1. The noise-free complex signal $c_k(\boldsymbol{x})$ measured by the k-th RSC at voxel $\boldsymbol{x}$ is proportional to the CSP $b_k(\boldsymbol{x})$ at that voxel [9];
2. The CSP $b_k(\boldsymbol{x})$ at voxel $\boldsymbol{x}$ is inversely proportional to the squared distance between the RSC position and $\boldsymbol{x}$ and, in that respect, is spatially smooth [4].
3. Drifts in the signal phase are introduced due to a number of factors: radiofrequency filtering, noncentered echo, readout compensation gradients and/or static field inhomogeneities and chemical shifts [6].
4. The covariance structure used for decorrelating the CSPs varies in time as pre-amplifiers in the RSCs heat up [7].
5. Motion and physiological noise obviously introduce dramatic distortions.

Properties 1-3 are helpful for designing a sound CSP estimator for Eq. (2) while properties 4-5 provide insights into what type of acquisitions is most suited for CSP estimation. Using properties 1-3, we define the CSP estimator using spatial smoothing and additional RBC data for phase normalization to mitigate phase-variation artifacts. For a proper mathematical definition, let us define:

$$\boldsymbol{\xi}(\boldsymbol{x}) = \sum_{j=1}^{|V|} W\left(\frac{\|\boldsymbol{x}_j - \boldsymbol{x}\|}{\tau}\right) \Sigma^{-1/2}\mathbf{c}(\boldsymbol{x}_j)\,, \tag{4}$$

where $W\left(\frac{\|\boldsymbol{x}_j-\boldsymbol{x}\|}{\tau}\right) = \left[\sum_{\ell=1}^{|V|} g\left(\frac{\|\boldsymbol{x}_\ell-\boldsymbol{x}\|}{\tau}\right)\right]^{-1} g\left(\frac{\|\boldsymbol{x}_j-\boldsymbol{x}\|}{\tau}\right)$, with Σ being the noise covariance structure estimator defined in Eq. (3). Likewise, let $\xi_0(\boldsymbol{x})$ be the same random variable defined from the RBC signals. Our CSP estimator can be formulated in the following terms:

$$\boldsymbol{\beta}(\boldsymbol{x}) = \frac{\xi_0^\star(\boldsymbol{x})}{\|\xi_0(\boldsymbol{x})\|} \cdot \frac{\boldsymbol{\xi}(\boldsymbol{x})}{\|\boldsymbol{\xi}(\boldsymbol{x})\|}\,. \tag{5}$$

The k-th component of the CSP estimator proposed in eq. (5) is the product of two complex-valued random variables. It can be expanded as:

$$\beta_k(\boldsymbol{x}) = \left[\mathrm{R}_0(\boldsymbol{x})\mathrm{R}_k(\boldsymbol{x}) + \mathrm{I}_0(\boldsymbol{x})\mathrm{I}_k(\boldsymbol{x})\right] + j\left[\mathrm{R}_0(\boldsymbol{x})\mathrm{I}_k(\boldsymbol{x}) - \mathrm{I}_0(\boldsymbol{x})\mathrm{R}_k(\boldsymbol{x})\right]\,, \tag{6}$$

where $\mathrm{R}_k(\boldsymbol{x}) := \mathcal{R}\left(\xi_k(\boldsymbol{x})\right) / \|\boldsymbol{\xi}(\boldsymbol{x})\|$ and $\mathrm{I}_k(\boldsymbol{x}) := \mathcal{I}\left(\xi_k(\boldsymbol{x})\right) / \|\boldsymbol{\xi}(\boldsymbol{x})\|$, $k \in [\![1, L]\!]$, and $\mathrm{R}_0(\boldsymbol{x})$ and $\mathrm{I}_0(\boldsymbol{x})$ are similarly defined as the real and imaginary parts of the normalized RBC-related variable ξ_0. Hence, determining the bias and variance of $\beta_k(\boldsymbol{x})$ reduces to determining the bias and variance of $\mathrm{R}_k(\boldsymbol{x})$.

2.3 Distribution of the Squared Norm of the CSP Estimator

The $\mathbb{C}^L$-valued random variable $\boldsymbol{\xi}(\boldsymbol{x})$ from Eq. (4) is a linear combination of multivariate complex Gaussian variables. Hence, in turn, $\boldsymbol{\xi}(\boldsymbol{x})$ is a multivariate Gaussian variable with mean and covariance given by:

$$\boldsymbol{\xi}(\boldsymbol{x}) := \sum_{j=1}^{|V|} W\left(\frac{\|\boldsymbol{x}_j - \boldsymbol{x}\|}{\tau}\right) \varSigma^{-\frac{1}{2}}\boldsymbol{c}(\boldsymbol{x}_j) \quad \text{and} \quad \mathrm{Cov}\left[\boldsymbol{\xi}(\boldsymbol{x})\right] := \sigma^2 \boldsymbol{I}_L\,,$$

with $\sigma^2 := \sum_{j=1}^{|V|} W^2\left(\frac{\|\boldsymbol{x}_j-\boldsymbol{x}\|}{\tau}\right)$. Now, observe that $\mathrm{R}_k^2(\boldsymbol{x}) = \frac{\mathrm{X}}{\mathrm{X}+\mathrm{Y}}$, where:

$$\mathrm{X} := \frac{\mathcal{R}\left(\xi_k(\boldsymbol{x})\right)^2}{\sigma^2} \quad \text{and} \quad \mathrm{Y} := \frac{1}{\sigma^2}\left[\mathcal{I}\left(\xi_k(\boldsymbol{x})\right)^2 + \sum_{\substack{\ell=1\\ \ell\neq k}}^{L}\left(\mathcal{R}\left(\xi_\ell(\boldsymbol{x})\right)^2 + \mathcal{I}\left(\xi_\ell(\boldsymbol{x})\right)^2\right)\right].$$

The real-valued random variables X and Y are independent and both formed of the sum of squared independent Gaussian variables. Hence, they both follow non-central χ^2-distributions, with respective degrees of freedom (DoF) $2\alpha_1 = 1$ and $2\alpha_2 = 2L - 1$ and non-centrality parameters (NcP) λ_1 and λ_2 given by:

$$\lambda_1 = \frac{\mathcal{R}\left(\xi_k(\boldsymbol{x})\right)^2}{\sigma^2} \quad \text{and} \quad \lambda_2 = \frac{1}{\sigma^2}\left[\mathcal{I}\left(\xi_k(\boldsymbol{x})\right)^2 + \sum_{\substack{\ell=1\\ \ell\neq k}}^{L}\left(\mathcal{R}\left(\xi_\ell(\boldsymbol{x})\right)^2 + \mathcal{I}\left(\xi_\ell(\boldsymbol{x})\right)^2\right)\right].$$

As a result, $\mathrm{R}_k^2(\boldsymbol{x})$ follows a **doubly non-central Beta** (DNcB) distribution [8] with DoFs $\alpha_1 = 1/2$ and $\alpha_2 = L - 1/2$ and NcPs λ_1 and λ_2, respectively.

2.4 Bias and Variance of the CSP Estimator

Let $T = \mathrm{R}_k^2(\boldsymbol{x})$, $\alpha^+ = \alpha_1 + \alpha_2$, $\lambda^+ = \lambda_1 + \lambda_2$ and $\theta_1 = \lambda_1/\lambda^+$. Since T a DNcB random variable, its first two raw moments are given by [8]:

$$\mathbb{E}(T) = \mathbb{E}\left(\frac{\alpha_1 + \theta_1 P}{\alpha^+ + P}\right), \mathbb{E}(T^2) = \mathbb{E}\left(\frac{\alpha_1(\alpha_1+1) + (2\alpha_1 + 2 - \theta_1)\theta_1 P + \theta_1^2 P^2}{(\alpha^+ + P)(\alpha^+ + 1 + P)}\right)$$

where P is a Poisson-distributed random variable with parameter $\lambda^+/2$. After some calculations, one can show that the above equations simplify to:

$$\begin{aligned} \mathbb{E}(T) &= \frac{\alpha_1}{\alpha^+ - 1} M\left(1, \alpha^+; -\frac{\lambda^+}{2}\right) + \frac{\theta_1\lambda^+}{2\alpha^+} M\left(1, \alpha^+ + 1; -\frac{\lambda^+}{2}\right), \\ \mathbb{E}\left(T^2\right) &= \frac{\theta_1^2\lambda^+}{2\alpha^+} M\left(1, \alpha^+ + 1; -\frac{\lambda^+}{2}\right) + \frac{\alpha_1(\alpha_1+1)}{(\alpha^+ - 1)\alpha^+} M\left(2, \alpha^+ + 1; -\frac{\lambda^+}{2}\right) \\ &\quad + \frac{(2(\alpha_1+1) - \theta_1(\alpha^+ + 1))\theta_1\lambda^+}{2\alpha^+(\alpha^+ + 1)} M\left(2, \alpha^+ + 2; -\frac{\lambda^+}{2}\right), \end{aligned} \tag{7}$$

where M denotes Kummer's confluent hypergeometric function [1]. Now, using the Taylor series expansion of the square root around $\mathbb{E}(T)$, we can show that:

$$\mathbb{E}(\mathrm{R}_k(\boldsymbol{x})) \approx \left[2\mathbb{P}\left(\mathrm{R}_k(\boldsymbol{x}) > 0\right) - 1\right] \frac{\sqrt{\mathbb{E}(T)}}{8}\left(9 - \frac{\mathbb{E}\left(T^2\right)}{\mathbb{E}(T)^2}\right), \tag{8}$$

where the probability of $\mathrm{R}_k(\boldsymbol{x})$ being positive can be analytically derived as:

$$\mathbb{P}\left(\mathrm{R}_k(\boldsymbol{x}) > 0\right) = \mathbb{P}\left(\mathcal{R}\left(\xi_k(\boldsymbol{x})\right) > 0\right) = G\left(\frac{\mathcal{R}\left(\xi_k(\boldsymbol{x})\right)}{\sigma}\right).$$

Equations (7) and (8) provide the first 2 raw moments of $\mathrm{R}_k(\boldsymbol{x})$. Similar equations for $\mathrm{I}_k(\boldsymbol{x})$, $\mathrm{R}_0(\boldsymbol{x})$ and $\mathrm{I}_0(\boldsymbol{x})$ can be straightforwardly obtained, which ultimately yields analytic expressions of bias and variance of the magnitude, real and imaginary parts of the CSP estimator $\beta_k(\boldsymbol{x})$ of k-th RSC proposed in Eq. (6).

In particular, the bias of $\beta_k(\boldsymbol{x})$ depends on the smoothing parameter τ and the initial SNRs $\|\Sigma^{-\frac{1}{2}}\boldsymbol{c}(\boldsymbol{x})\|$. Hence, given initial SNRs, the smoothing parameter τ can be optimized in order to guarantee minimally biased CSP estimates.

3 Experiments

3.1 Study of Bias and Variance of Our CSP Estimator

The goal of this simulation is to assess the behavior of the CSP estimator magnitude upon variation of the smoothing parameter τ and the SNR ρ_0 of the RSoS image formed from noise-free complex data. We generated a 33×33 2D image centered in the voxel of interest with SNR ρ_0, attributing decreasing SNRs to the surrounding voxels proportionally to their distance in pixel units to the center voxel. We simulated an array of 32 RSCs uniformly located on the image anti-diagonal, with different uniform phases and magnitude inversely proportional to the distance between the RSC and the voxel of interest. We used a Gaussian kernel of standard deviation τ for smoothing. We assessed evolution of bias and variance of the magnitude of our CSP estimator proposed in Eq. (5) by evaluating numerically the analytic expressions provided in Eqs. (6) to (8). We plotted them against ρ_0 and τ and investigated the optimal smoothing $\tau^\star$ that minimizes the bias of our CSP estimator as a function of initial SNR ρ_0.

3.2 Application to the MR Reconstruction Problem

We applied our CSP estimator for imaging a healthy volunteer at 0.4 mm isotropic. We targeted a T1 MPRAGE image and we imaged the subject with a 3T Siemens Skyra MR scanner. We additionally acquired an independent set of low-resolution (2 mm iso) RSC and RBC images for CSP estimation. The SNR for the RSC images was around 40 dB, which, according to the theory, requires a spatial smoothing of $\tau = 1.5$ mm. Additionally, we also estimated the CSPs using [3]'s method (Siemens prescan normalize). We compare the uncorrected high resolution reconstruction to the ones obtained after intensity inhomogeneity correction (IIC) using both sets of CSP estimates ([3]'s and our optimized one). Quantitatively, we use sharpness measures (image energy M1, gradient magnitude energy M2) to compare the results, for which higher values highlight a better reconstruction.

4 Results

4.1 Study of Bias and Variance of our CSP Estimator

Figure 1a shows the relative bias and the variance of the magnitude of our CSP estimator as a function of the smoothing parameter τ for different SNRs. The first result is that the variance decreases as the amount of smoothing and SNR increase as expected. The two most important messages from Fig. 1a however

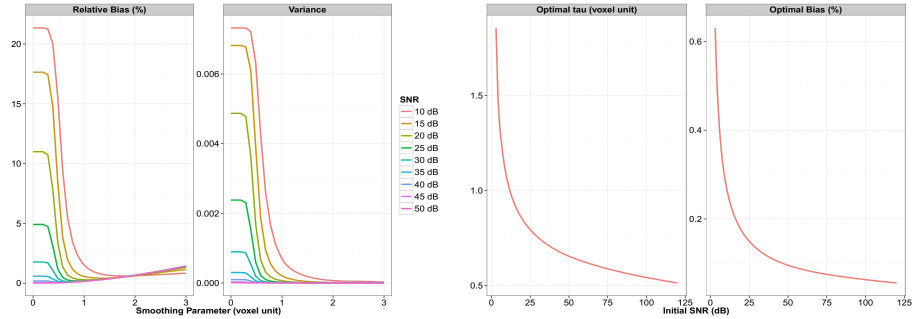

(a) (b)

Fig. 1. Bias and Variance of Magnitude of CSP Estimator. (a) bias and variance of the magnitude of the CSP estimator as defined in Eq. (5); (b) optimal smoothing parameter as a function of the initial SNR and corresponding value of minimal bias.

are that (i) smoothing does not systematically either introduce bias or reduce bias but there is an optimal degree of smoothness that yields minimal bias, which depends on the SNR. Figure 1b further investigates this phenomenon by plotting the optimal degree of smoothness and corresponding minimal bias against the SNR. If the initial images used for CSP estimation already have high SNR, smoothing will introduce bias in the CSP estimates whereas, if they have low SNR, there is a optimal smoothing that ensures minimally biased CSPs.

4.2 Application to the MR Reconstruction Problem

Figure 2 shows an axial slice of a high resolution brain MPRAGE reconstruction achieved using a SENSE1 reconstruction according to Eq. (1). Image (a)

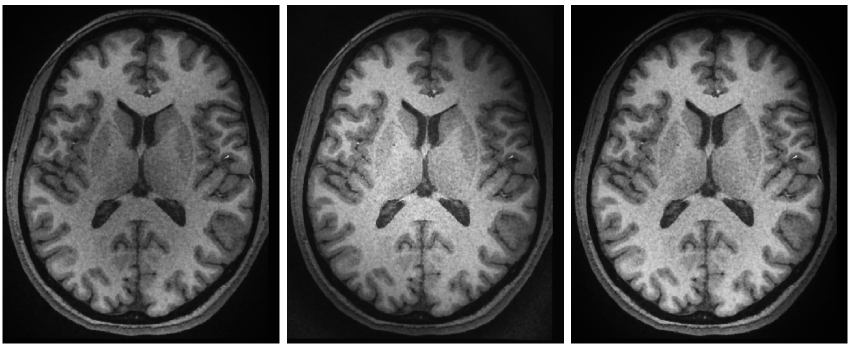

(a) $M1 = 4.98$, $M2 = 2.7e7$ (b) $M1 = 4.43$, $M2 = 1.8e7$ (c) $M1 = 6.56$, $M2 = 3.3e7$

Fig. 2. High Resolution brain MPRAGE reconstruction. Image reconstruction according to Eq. (1) with (a) no IIC, (b) IIC using [3]'s CSPs, (c) IIC using our CSPs.

is obtained with no IIC, which clearly depicts the loss of signal in the center of the image. Image (b) illustrates pre-scan normalization, where we can see an undesirable loss (resp., amplification) of signal in the upper right (resp., middle left) area. Image (c) displays the IIC from our minimally biased CSPs, which is uniform in sensitivity as desired. Sharpness measures M1 and M2 quantitatively confirms the improvement obtained using our CSP estimates.

5 Discussion

In this paper, we generalized the CSP estimator proposed in [3] to infer complex-valued CSP estimates. This estimator uses spatial smoothing and additional body coil data for phase normalization to mitigate phase-variation artifacts.

The main contribution is the derivation of the statistical distribution of our proposed estimator. This allows us to establish that, in order to achieve minimally biased CSP estimates, (i) there is an optimal degree of smoothing that depends on the image SNR and (ii) high SNR in the images used for CSP estimation is highly recommended. In addition, from MR physics considerations, it is even more recommended to acquire low spatial resolution data to keep the acquisition time short and thus avoid the problem of time-varying covariance structures and mitigate motion and physiological noise. To the best of our knowledge, this is the first study that propose a detailed understanding of a CSP estimator. It is shown to resolve intensity inhomogeneities in structural images and to present a significant improvement over the on-line scanner pre-scan normalization, especially for high spatial resolution image reconstructions (in which case, CSPs are still estimated from an independent low-resolution scan).

References

1. Abramowitz, M., Stegun, I.: Handbook of Mathematical Functions: With Formulas, Graphs, and Mathematical Tables. Applied maths, Dover Publications (1964)
2. Blaimer, M., Breuer, F., Mueller, M., Heidemann, R.M., Griswold, M.A., Jakob, P.M.: SMASH, SENSE, PILS, GRAPPA: how to choose the optimal method. Top. Magn. Reson. Imaging 15(4), 223–236 (2004)
3. Brey, W.W., Narayana, P.A.: Correction for intensity falloff in surface coil magnetic resonance imaging. Med. Phys. 15(2), 241–245 (1988)
4. Haacke, E., et al.: Magnetic Resonance Imaging: Physical Principles and Sequence Design, 1st edn. Wiley-Liss (1999)
5. Keil, B., Wald, L.L.: Massively parallel MRI detector arrays. J. Magn. Reson. 229(6), 75–89 (2013)
6. McVeigh, E.R., Bronskill, M.J., Henkelman, R.M.: Phase and sensitivity of receiver coils in magnetic resonance imaging. Med. Phys. 13(6), 806–814 (1986)
7. McVeigh, E., Henkelman, R., Bronskill, M.: Noise and filtration in magnetic resonance imaging. Med. Phys. 12(5), 586 (1985)
8. Ongaro, A., Orsi, C.: On non-central beta distributions. In: Cabras, S., Di Battista, T., Racugno, W. (eds.) 47th SIS Sci. Meet. Ital. Stat. Soc. (2014)
9. Roemer, P., et al.: NMR phased array. Magn. Reson. Med. 16(2), 192–225 (1990)
10. Vovk, U., Pernuš, F., Likar, B.: A review of methods for correction of intensity inhomogeneity in MRI (2007)